Spiral and circular waves in the flow between a rotating and a stationary disk

L. Schouveiler, P. Le Gal, M. P. Chauve

Institut de Recherche sur les Phénomènes Hors Equilibre
U.M.R 138 CNRS - Universités Aix-Marseille I & II
12, Avenue du Général Leclerc, 13003 Marseille, France

Y. Takeda

Laboratory for Spallation Neutron Source
Paul Scherrer Institute
CH-5232 Villigen PSI, Switzerland

ABSTRACT

Circular and spiral waves are observed in the flow between a rotating and a stationary disk. These waves are generated by instabilities of the stationary disk boundary layer. This experimental work is then devoted to their study by means of flow visualisations and measurements of the associated velocity fields. In particular, instantaneous velocity profiles are measured by ultrasonic Doppler anemometry. The spatio-temporal characteristics of the waves are studied with the help of Fourier transforms of these velocity signals.

List of symbols

A_c, A_s	amplitudes of respectively the circular and the spiral waves
f_c, f_s	frequencies of respectively the circular and the spiral waves
h	axial distance between the two disks
N	rotation frequency of the rotating disk
P1, P2	UDA probe positions
R	radius of the disks
$Re_R = \Omega R^2/\nu$	Reynolds number
t	time
$v_\xi(\xi,t)$, $\langle v_\xi(\xi)\rangle$	instantaneous and mean profiles of the velocity projection on the ξ axis
$v_r(r,t)$, $\langle v_r(r)\rangle$	instantaneous and mean profiles of the radial velocity
(r,θ,z)	cylindrical coordinate system
ε	orientation angle of the spiral waves
$\gamma = h/R$	aspect ratio
$\Omega = 2\pi N$	angular velocity of the rotating disk
ξ	coordinate along the ultrasonic beam axis

1
Introduction

In a previous exprimental study (Schouveiler *et al.* 1996), we showed that the flow between a rotating and a stationary coaxial parallel disk in a fixed casing, exhibits different instabilities according to the value of the distance between the two disks and to the angular velocity of the rotating disk. Some aspects of such instabilities have already been reported in the earlier experimental works of San'kov and Smirnov (1984), Itoh (1988) and Sirivat (1991).

In this paper, we describe the flow regimes which appear when the distance between the two disks is much larger than the thickness of the two disk boundary layers and for moderate Reynolds numbers. In this case, we observe two coexisting traveling waves that appear near the stationary disk. As expected, the flow pattern resulting from the interaction of these systems becomes more and more complex when the Reynolds number is increased. First, visualizations of the flow patterns are realized. Then, an ultrasonic Doppler anemometer is used to quantify the spatio-temporal behavior of the flow. This new type of anemometer permits to measure instantaneous velocity profiles and a spectral analysis of the obtained space-time velocity signals are realized with the help of the Fourier transform.

2
Experimental details

2.1
Experimental apparatus and procedure

The experimental setup is schematically shown in Fig. 1. It consists of a stainless steel horizontal rotating disk, of radius $R = 140$ mm , driven at a variable speed by an electrical motor. The rotation frequency N is measured with an optical encoder. This disk is set in a vertical cylindrical housing with a sliding fit so that there is no radial gap between the vertical cylindrical wall and the edge of the disk. The top of the housing, constituting the stationary disk, is made of Plexiglas to permit flow visualization. The system is completely filled with tap water at ambient temperature. The height of the rotating disk inside the housing is adjustable in such a way that the axial distance h between the two parallel disks can be continuously varied from 1 to 20 mm.

A cylindrical coordinate system (r, θ, z) is defined with the z axis coinciding with the axis of rotation and with its origin located at the center of the stationary disk. The control

parameters of this flow are the aspect ratio $\gamma = h/R$ and the Reynolds number $Re_R = \Omega R^2/\nu$, where $\Omega = 2\pi N$ is the angular velocity of the rotating disk and ν the kinematic viscosity of water.

In the present study, the distance h is fixed to 16 mm ($\gamma = 11.43 \times 10^{-2}$) and N is first increased from 0.1 to 0.6 Hz (or rotation per second) by steps of 0.02 Hz, then decreased back in the same manner. Thus the Reynolds number Re_R is varied in the range 12.3×10^3 to 73.9×10^3.

2.2

Experimental techniques

The patterns of the different flow regimes are visualized by adding a small amount of flake particles to the working fluid. These particles have a high reflective index and they tend to align themselves along stream surfaces, thus becoming visible under appropriate lighting conditions (for further details on this visualization technique, see Savas(1985)). The flow patterns are filmed, through the stationary disk, with a video camera located above the stationary disk on the rotation axis (Fig. 1).

The velocity field has been measured with an Ultrasonic Doppler Anemometer (UDA). This device, working with a pulsed ultrasonic emission, allows the measurement of instantaneous profiles of the velocity component projected onto the ultrasound beam direction. The working fluid is seeded with nylon spherical microparticles having a diameter of 80 µm and a density of 1.02 g/cm^3. This apparatus, working alternately in emitter and receiver, detects the Doppler frequency shift of the ultrasound beam which is reflected by these particles in suspension in the flow. Thus, instantaneous velocity profiles can be recorded as a function of time. In our case, the space resolution of this method is 0.74 mm along the ultrasonic beam and 2.5 mm or 5 mm in the transversal direction. The profile acquisition frequency is either 9.35 Hz or 7.39 Hz. For more details on the UDA method, see Takeda *et al.* (1993).

In order to measure different components of the velocity field, the UDA piezoelectric probe has been placed along two typical axis ; P1 for radial profiles and P2 for axial profiles. These two positions (P1 and P2) of the UDA probe are given in Fig. 2. In position P1, the UDA probe and then the ultrasonic beam are parallel to a radius of the disks at a distance of 7 mm from the stationary disk. In this case, we measure, with the 2.5 mm transversal resolution, instantaneous radial velocity profiles along a radius : $v_r(r,t)$. For position P2, the probe is placed in a azimuthal plane defined by a constant radius r, and makes an angle of 20°

versus the vertical axis. This angle has been chosen large enough to minimize the echo due to the rotating disk and small enough to minimize the reflections on the different interfaces. For P2, we define a local coordinate ξ (Fig. 2) along the ultrasonic beam with its origin on the stationary disk. ξ is scaled by $h/\cos 20°$ so that it is equal to 1 on the rotating disk. In this case, the measured profiles $v_\xi(\xi,t)$ of the velocity projection onto the ξ axis reveal the axial structure of the flow.

3
Results

3.1
Basic flow

The characteristic features of these types of rotating flows can be found in the extensive review of Zandbergen and Dijkstra (1987). For the values of γ and Re_R used in the present investigation and outside the boundary layer of the vertical housing, the stationary axisymmetrical basic flow is of Batchelor type. We recall that this flow consists of two boundary layers, one on each disk, separated by an inviscid rotating core where the tangential component of the velocity is constant and the radial component is zero. The main features of this Batchelor flow are recovered on the temporal mean profiles $\langle v_\xi(\xi) \rangle$ which will be presented later in Fig. 5.a and 6.a.

3.2
Visualization

The primary instability of the Batchelor basic flow occurs in the boundary layer of the stationary disk which is more unstable than the rotating one, in accordance with the experimental and numerical studies of Itoh (1988, 1991). When N is close to 0.1 Hz (for $\gamma = 11.43 \times 10^{-2}$) this instability gives rise to the formation of traveling circular vortices (Fig. 3). These vortices are formed near the periphery of the disk and move towards the center. Such traveling circular structures have also been reported, in similar experiments, by Itoh (1988), more recently by Gauthier and Rabaud (1996), and in the numerical simulations of Cousin-Rittemard (1996). They have also been observed by Savas (1983, 1987) in an experimental study of the transient regimes of the boundary layer over a stationary disk in a

rotating fluid (Bödewadt layer). As they travel towards the center, we observe pairings of vortices in such a way that the frequency corresponding to this circular wave system varies along a radius. Similar observations of frequency variation have also been made in the numerical studies of Cousin-Rittemard (1996) and of Lopez (1996) for transient Bödewadt layer flows. This point will be quantitatively investigated by the measurements presented in § 3.3.

As the angular velocity Ω is increased, a second system of waves, constituted by 16 spiral vortices, appears in the peripheral area together with the circular ones (Fig. 4). These spirals possess an angle $\varepsilon \approx 25°$, where ε is defined, in accordance with the terminology of Sirivat (1991), as the angle between the vortex axis and the azimuthal direction, positively counted in the rotation sense of the disk. They are non stationary and, contrary to the circular waves, travel outwards. This kind of traveling spiral waves is only reported in the experimental study of Itoh (1988).

3.3

Anemometry

In this part, we present the results of the UDA measurements realized for an experimental series when Re_R is increased. The raw velocity fluctuation data, obtained by subtraction of the temporal mean profile from the instantaneous profiles, and/or the filtered velocity fluctuation data, obtained by using frequency windows in order to eliminate the experimental noise, are displayed. The values of these spatiotemporal velocity signals and of the corresponding temporal power spectra are coded with gray levels in the space-time plane, respectively in the space-frequency plane.

For flow parameter values for which the two wave systems coexist (see e.g. Fig. 4), UDA measurements with the P2 probe position have been realized at two different radii $r = 70$ and 120 mm in order to determine the axial structure of the flow disturbed respectively by the circular vortex system (central area) and by the spiral vortex system (peripheral area). At these radii and for $Re_R = 23.4 \times 10^3$ (N = 0.19 Hz), the temporal mean profiles $\langle v_\xi(\xi) \rangle$ are displayed in Fig. 5.a and 6.a. We recall that the ξ coordinate is equal to 0 on the stationary disk and to 1 on the rotating one. The axial component of the velocity being small in comparison with the tangential one, the features of the tangential velocity of the Batchelor flow are clearly recovered on these mean profiles. Thus, we can distinguish two boundary

layers (one on each disk) separated by a central core in which the gradient, versus ξ, of the velocity is nearly zero. For the same parameter values, Fig. 5.b and Fig. 6.b present the filtered signals of the velocity fluctuations $v_\xi(\xi,t)-\langle v_\xi(\xi)\rangle$ respectively in the circular waves ($r = 70$ mm) and in the spiral waves ($r = 120$ mm). Although the fluctuation amplitude is quite small, the periodic passages of the circular and spiral vortices are revealed by the gray encoding of the measurements. In both cases, these vortical structures located close to the stationary disk appear periodically in time (for $\xi < 0.5$) as alternate dark and light zones. The temporal power spectra of these fluctuations show one frequency peak called f_c for the circular waves and f_s for the spiral waves. The amplitude distributions along ξ of these temporal Fourier modes of frequencies f_c and f_s, referred as $A_c(\xi)$ and $A_s(\xi)$, are displayed in Fig. 5.c and 6.c. Both curves show clearly that the circular and spiral modes are located near the stationary disk. The distribution $A_s(\xi)$ (Fig. 6.c) presents one maximum at $\xi \approx 0.2$, contrary to $A_c(\xi)$ (Fig. 5.c) which vanishes at $\xi \approx 0.25$ which separates two maxima. Accordingly, we can see on the velocity fluctuation signals of Fig. 5.b, a layer around $\xi = 0.25$ where the fluctuations are nearly zero and which divides the perturbated area in two zones of same frequency f_c but with a phase difference close to π. Thus, the circular waves appear to be formed by a pair of vortical structures superposed on top on each other. Some visualizations of the flow in a radial plane realized by laser tomography (not presented here) confirm the existence of this double layer structure.

The raw and filtered velocity fluctuations of the radial velocity $v_r(r,t)-\langle v_r(r)\rangle$ in the external half of the flow ($r > 75$ mm) are displayed for two different Re_R in Fig. 7 and 8. These measurements are obtained with the P1 probe position. In Fig. 9, we present the temporal mean profile of radial velocity $\langle v_r(r)\rangle$ corresponding to the signal of Fig. 7 ($Re_R = 17.2\times10^3$). This mean profile shows the existence of a recirculation eddy at the periphery of the disk, near the stationary vertical side wall. This stationary recirculation eddy extends up to the point where the change of sign of the radial velocity occurs, here at around 135 mm. Such a recirculation has also been detected by Oliveira *et al.* (1982) in the case of an open rotating system. Vizualisations by laser tomography in a radial plane has confirmed the existence of this recirculation zone which radial extension decreases with Re_R.

On Fig. 7, the velocity fluctuation signal shows the circular vortices for $Re_R = 17.2 \times 10^3$ (N = 0.14 Hz). These vortices appear near the periphery ($r \approx 135$ mm) travel towards the center with a decreasing phase velocity. For the considered case of Fig. 7, this traveling velocity evolves from 10 mm/s near the periphery to 4 mm/s at a radius of 80 mm. Then, we can see periodic pairings of two vortices on three which occur at a radius r of around 95 mm. Therefore, at this radius we see the disappearing of one vortex on three. At a smaller radius, $r < 75$ mm (outside the measure area), secondary pairings that merge vortices two by two this time, have been observed by flow visualization. These pairings appear as space-time dislocations of the flow patterns as it can be verified on Fig. 7 at a radius $r \approx 95$ mm. On the corresponding power spectrum (Fig. 10) the dominating frequency f_c associated with these traveling cirular waves is, for $r > 95$ mm, equal to 0.42 Hz. This value is exactly three times the rotation frequency N of the disk. Then, for $r < 95$ mm, f_c is equal to twice the rotation frequency N. For radii less than 85 mm, the level of noise in the signal is too important to distinguish the frequency peaks which lead to secondary pairings and finally to $f_c = N$.

The velocity fluctuation signal of Fig. 8 shows, for $Re_R = 34.5 \times 10^3$ (N = 0.28 Hz), the coexistence of the two wave systems : the circular waves for $r < 105$ mm and the spiral ones for $r > 105$ mm. The opposite slopes of the traces of these two wave systems confirm the opposite sign of their radial phase velocity. Due to the frequency difference between the two wave systems, periodic dislocations occur at a radius around 105 mm, as it can be observed for t between 20 s and 30 s. The corresponding power spectrum is presented in Fig. 11. Now, the circular waves appear for a smaller radius than previously (Fig. 7), and at a frequency $f_c = 0.56$ Hz $= 2N$. We distinguish in the peripheral area ($r > 105$ mm) a peak at $f_s = 0.59$ Hz, clearly different and slightly higher than the frequency $f_c = 2N$ and corresponding to the traveling spiral vortices. The evolution with the rotation frequency N of dominating frequency f_s in the external area, associated with these spiral vortices, is displayed in Fig. 12. By comparing these evolutions for experimental series with increasing (O) and decreasing (+) N, we can see a significant difference at the same N. Thus, this diagram shows obviously a hysteresis in the spiral wave mode. We observe also frequency jumps, at N between 0.28 and 0.30 Hz for increasing N or between 0.31 and 0.29 Hz and between 0.23 and 0.21 Hz for decreasing N. These jumps separate N ranges where f_s evolves quasi-linearly

with N and which could correspond to changes of the number of spiral vortices on the disk circumference.

When the rotation frequency is further increased, we observe at the periphery of the disk, the appearance of new frequency peaks, as it can be seen in Fig. 13 for $Re_R = 39.4 \times 10^3$ (N = 0.32 Hz). Then, at higher Reynolds numbers, the number of peaks in the power spectra continues to increase, and the whole flow becomes more and more complex up to its turbulent state.

4

Conclusion

This experimental study shows that the flow between a rotating and a stationary disk shrouded by a stationary cylindrical housing is, at least in the central part, of Batchelor type in the sense that it consists of two boundary layers, one on each disk, separated by a core in which the azimuthal velocity is constant. At the periphery of the disks, we observe also the presence of a recirculation eddy. This circular roll may play a role in the destabilization of the whole flow. For the aspect ratio value considered here, the primary instability occurs near the stationary disk. It gives rise to the formation of a traveling vortex system constituted by double layer circular structures. The frequency f_c associated with this system is locked on the rotation frequency N of the rotating disk. In fact, it evolves from 3N at the periphery, to 2N for intermediate radii and finally to N near the center of the disk. These changes in frequency occur via pairings of vortices. It is noteworthy that such a frequency variation, with the same frequency ratios (1, 2/3 and 1/3), has also been observed in the numerical simulations of Cousin-Rittemard (1996), for axisymmetrical instability modes traveling in a toric cavity. When the Reynolds number is increased, a secondary instability occurs in the form of a traveling spiral vortex system located near the stationary disk. We show that the selection of the mode associated with these traveling spiral vortices is subject to a significant hysteresis. Moreover, jumps are observed in the evolution with the rotation frequency N of the corresponding frequency f_s. These frequency jumps could result from discrete changes of the number of spirals present on the disk, due to an Eckhaus instability.

References

Cousin-Rittemard N (1996) Contribution à l'étude des instabilités des écoulements axisymétriques en cavité inter-disques de type rotor-stator. Thèse de Doctorat, Université Paris VI

Gauthier G; Rabaud M (1996) Pivate communication

Itoh M (1988) Instability and transition of the flow around a rotating disk in a casing. Toyota Report 36: 28-36 (in Japanese)

Itoh M (1991) On the instability of flow between coaxial rotating disks. ASME Boundary Layer Stability and Transition to Turbulence, FED 114: 83-89

Lopez JM (1996) Flow between a stationary and a rotating disk shrouded by a co-rotating cylinder. Phys Fluids 8 (11): 2605-2613

Oliveira L; Bousgarbiès JL; Pécheux J (1982) Etude expérimentale de l'écoulement entre un disque fixe et un disque tournant. C R Acad Sc Paris 294 Série II: 1163-1165 (in French)

Savas Ö (1983) Circular waves on a stationary disk in a rotating flow. Phys Fluids 26: 3445-3448

Savas Ö (1985) On flow visualization using reflective flakes. J Fluid Mech 152: 235-248

Savas Ö (1987) Stability of Bödewadt flow. J Fluid Mech 183: 77-94

San'kov PI; Smirnov EM (1984) Bifurcation and transition to turbulence in the gap between rotating and stationary parallel disks. Fluid Dyn 19 (5): 695-702 (Original article in Russian (1984) Izv Akad Nauk SSSR, Mekh Zhidk Gaza 5: 28-36)

Schouveiler L; Le Gal P; Chauve MP; Takeda Y (1996) Experimental study of the stability of the flow between a rotating and a stationary disk. In : Advances in Turbulence VI. Gavrilakis S et al. (eds.): 385-388, Kluwer Academic Publishers

Sirivat A (1991) Stability experiment of flow between a stationary and a rotating disk. Phys Fluids A 3 (11): 2664-2671

Takeda Y; Fisher WE; Sakakibara J; Ohmura K (1993) Experimental observation of the quasiperiodic modes in a rotating Couette system. Phys Rev E 47: 4130

Zandbergen PJ; Dijkstra D (1987) Von Kármán swirling flows. Ann Rev Fluid Mech 19: 465-491

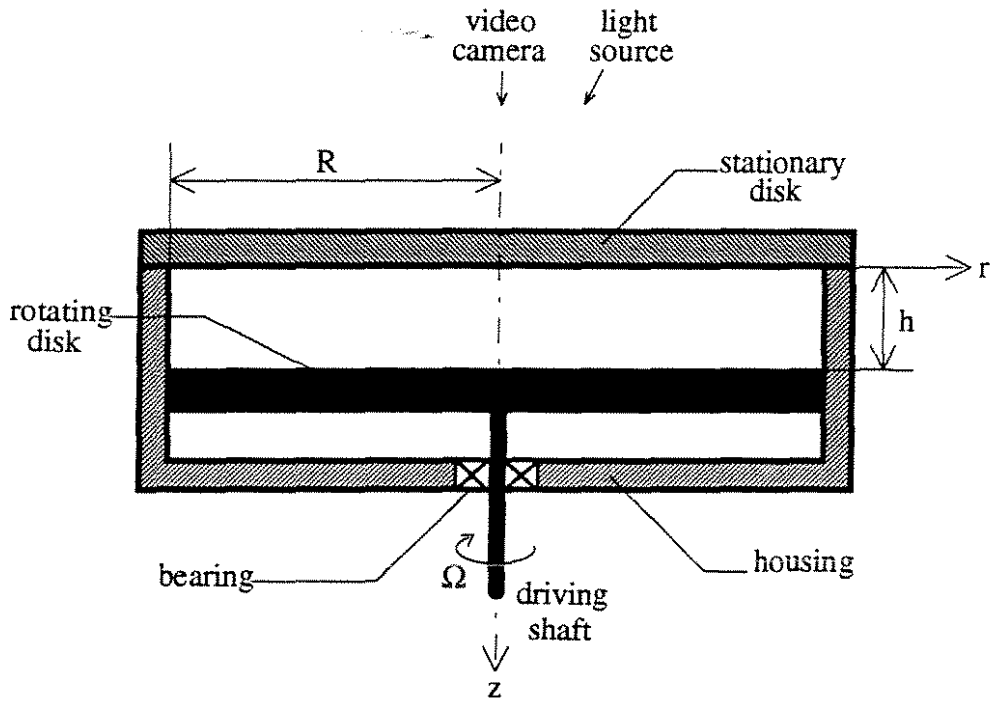

Fig. 1. Experimental apparatus

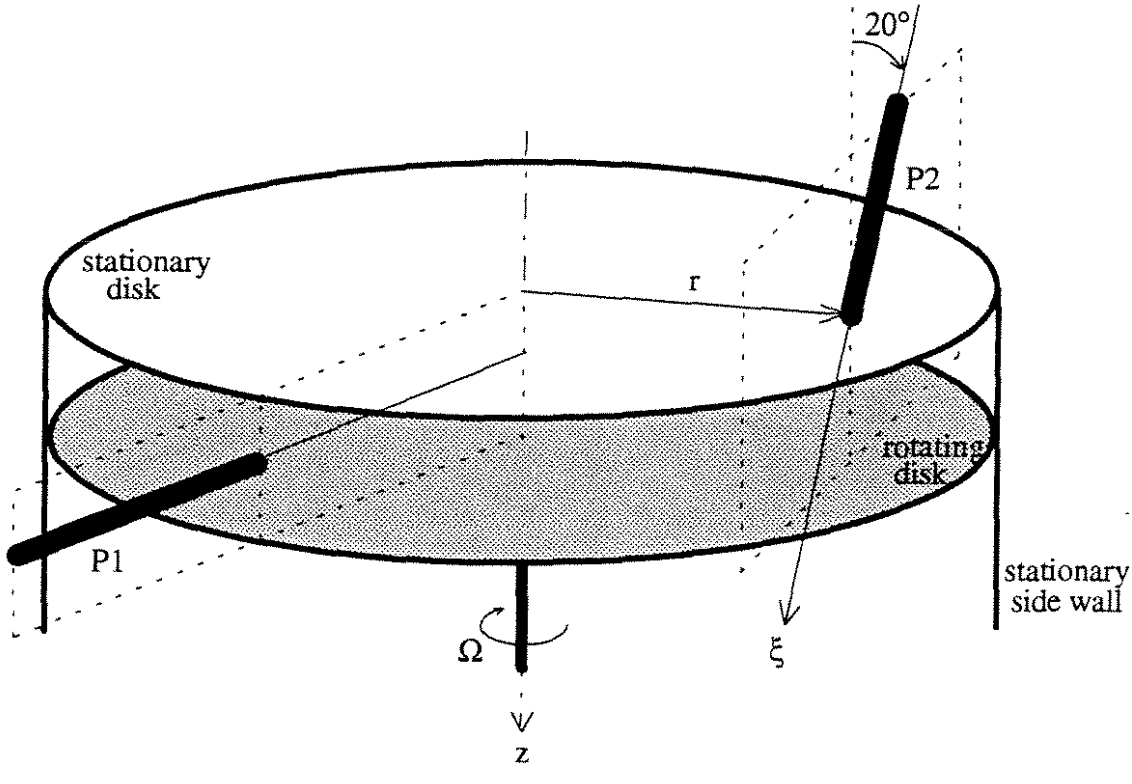

Fig. 2. UDA probe positions

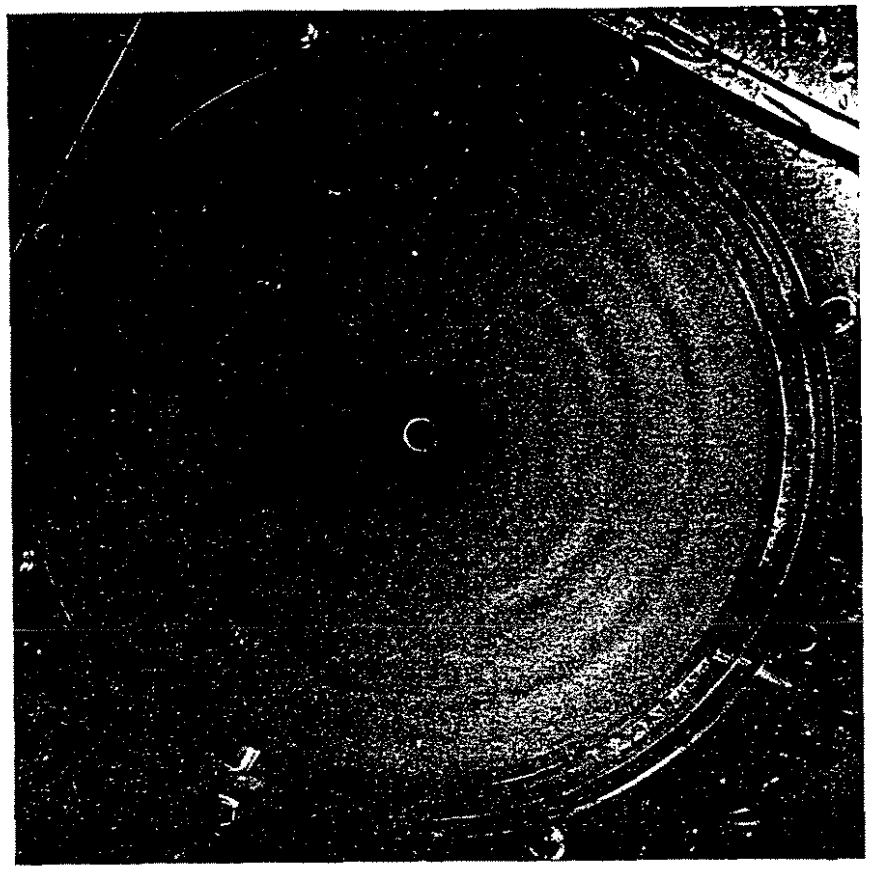

Fig. 3. Flow visualization : $\gamma = 11.43 \times 10^{-2}$, $Re_R = 16 \times 10^3$, $N = 0.13$ Hz. Clockwise rotation.

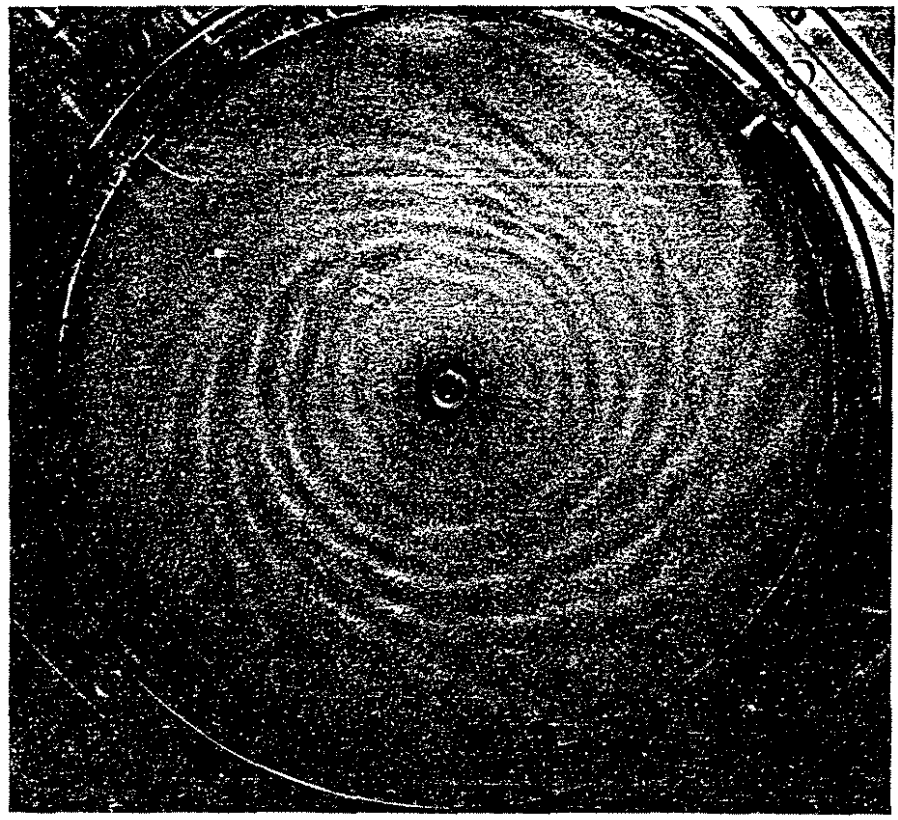

Fig. 4. Flow visualization : $\gamma = 11.43 \times 10^{-2}$, $Re_R = 28.3 \times 10^3$, $N = 0.23$ Hz. Clockwise rotation.

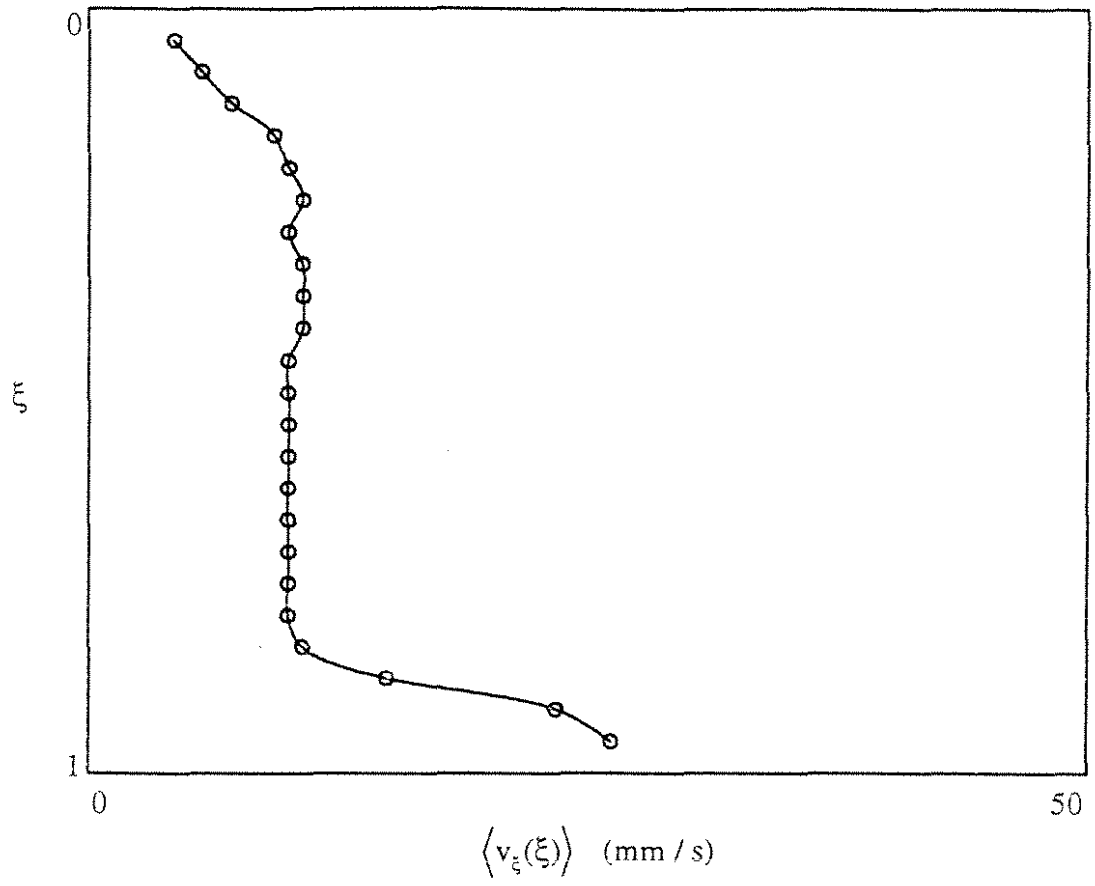

Fig. 5. $\gamma = 11.43 \times 10^{-2}$, $Re_R = 23.4 \times 10^3$, N = 0.19 Hz, r/R = 0.5. a. Temporal mean profile : $\langle v_\xi(\xi) \rangle$.

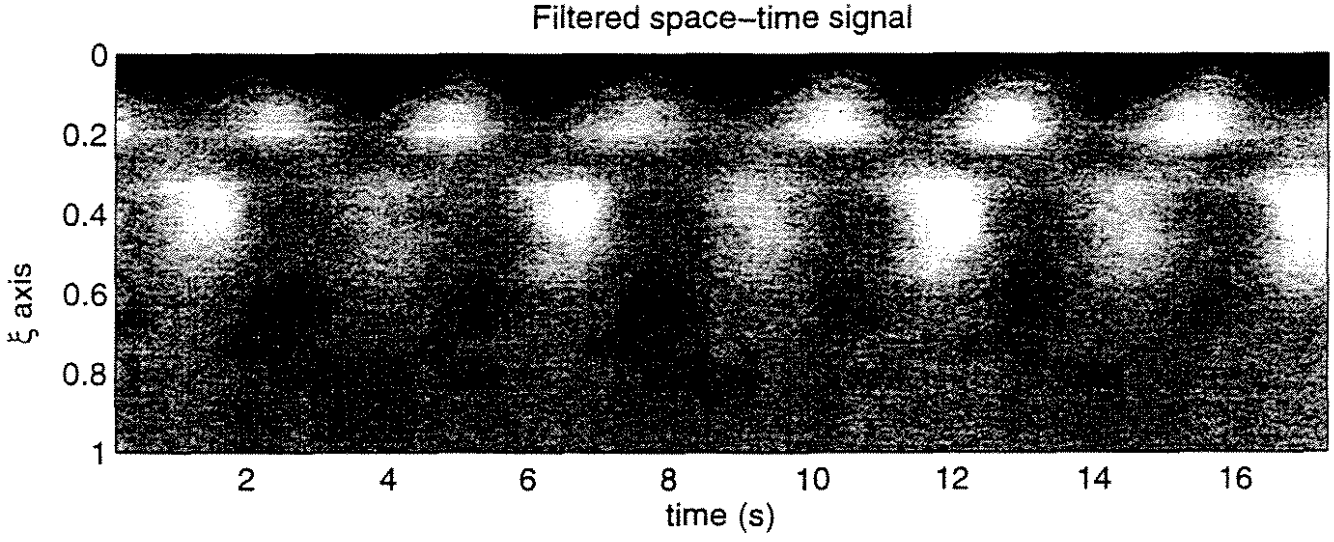

Fig. 5. $\gamma = 11.43 \times 10^{-2}$, $Re_R = 23.4 \times 10^3$, N = 0.19 Hz, r/R = 0.5. b. Filtered signal : $v_\xi(\xi, t) - \langle v_\xi(\xi) \rangle$.

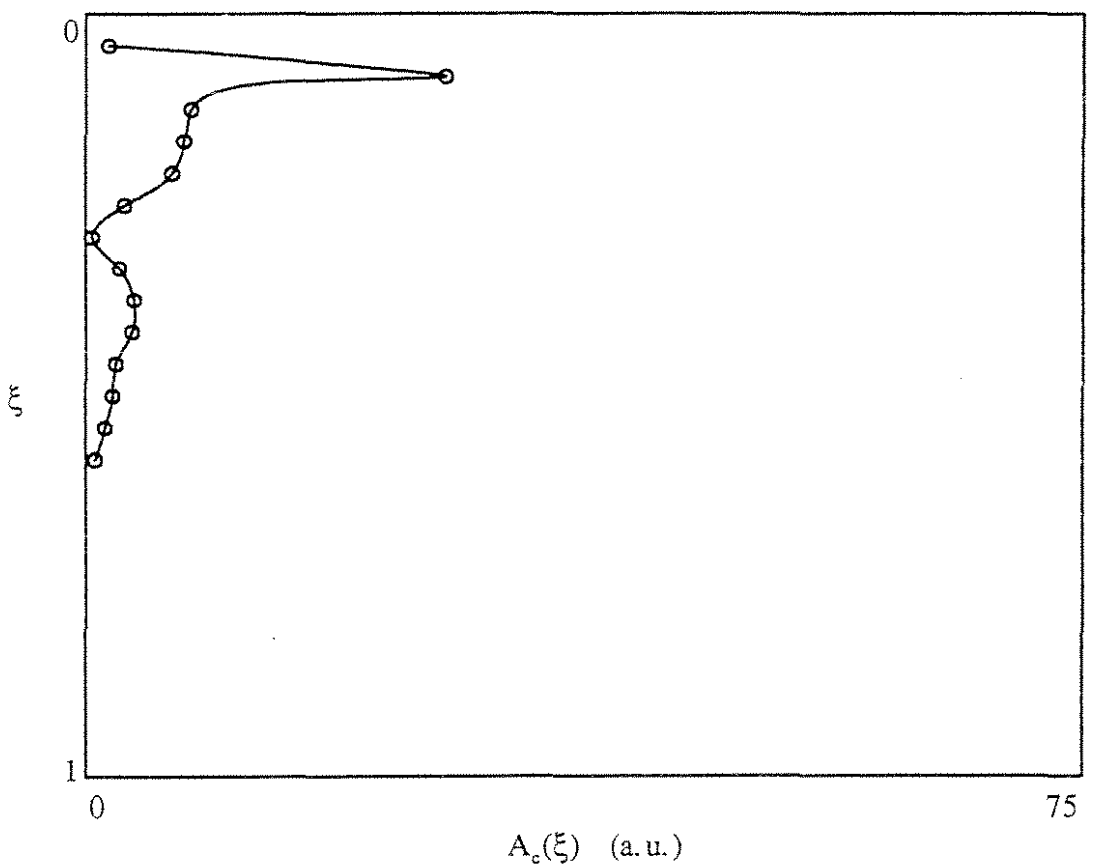

Fig. 5. $\gamma = 11.43 \times 10^{-2}$, $Re_R = 23.4 \times 10^3$, $N = 0.19$ Hz, $r/R = 0.5$. c. Amplitude $A_c(\xi)$ of the f_c Fourier mode.

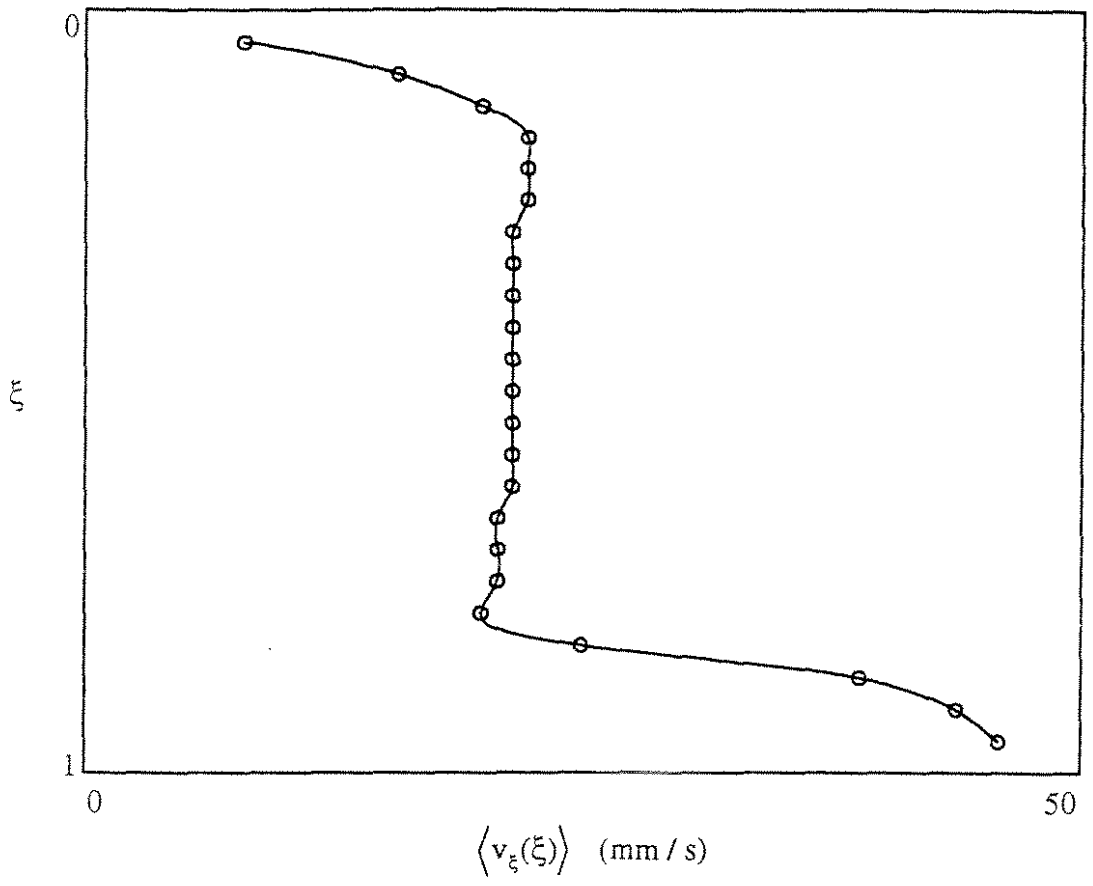

Fig. 6. $\gamma = 11.43 \times 10^{-2}$, $Re_R = 23.4 \times 10^3$, N = 0.19 Hz, r/R = 0.86.

a. Temporal mean profile : $\langle v_\xi(\xi) \rangle$.

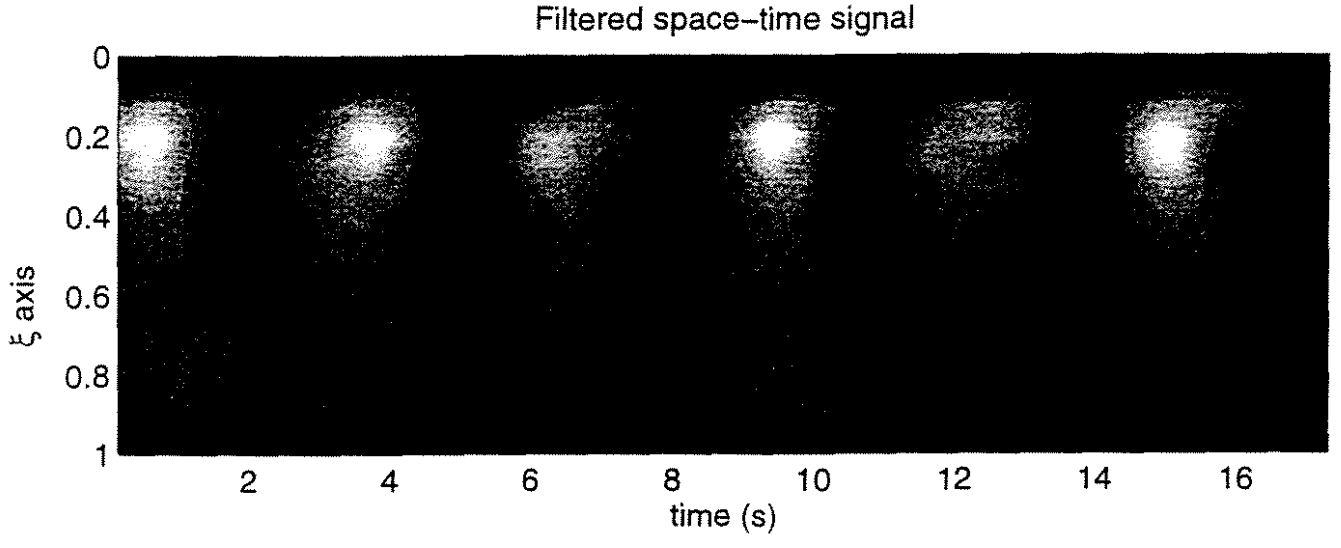

Fig. 6. $\gamma = 11.43 \times 10^{-2}$, $Re_R = 23.4 \times 10^3$, N = 0.19 Hz, r/R = 0.86.

b. Filtered signal : $v_\xi(\xi, t) - \langle v_\xi(\xi) \rangle$.

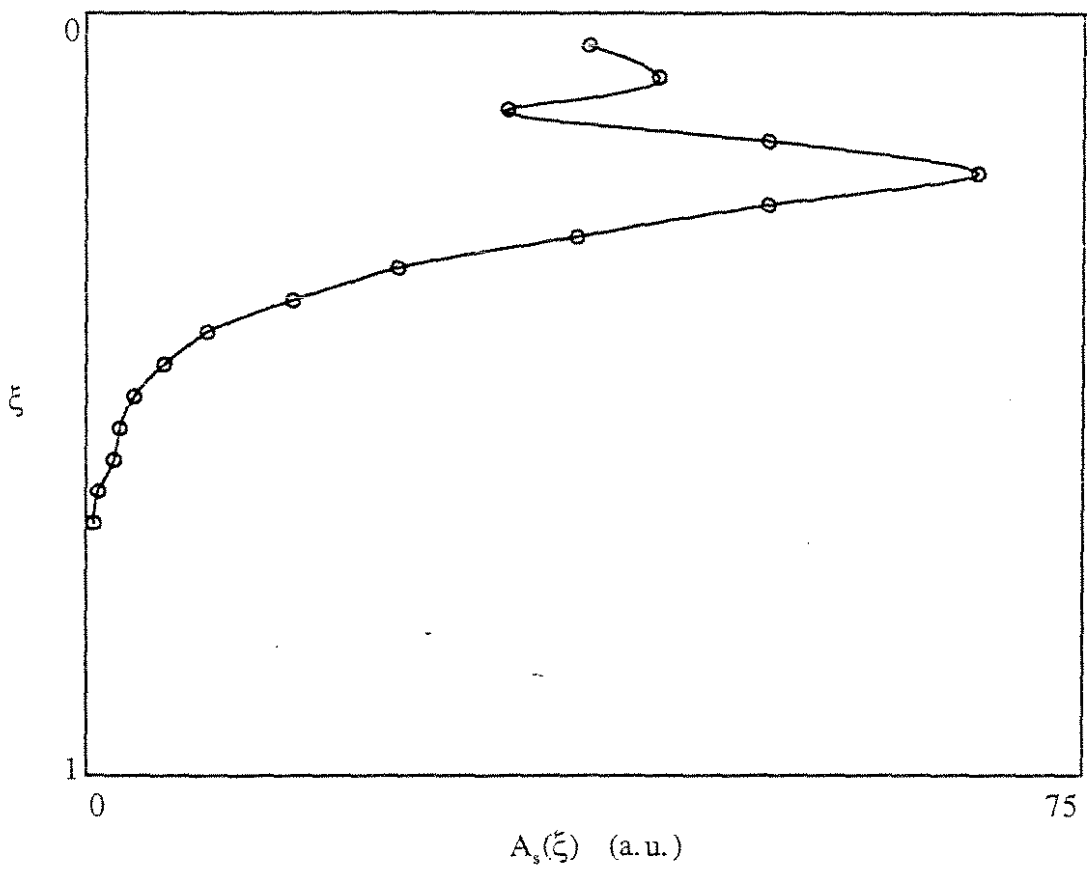

Fig. 6. $\gamma = 11.43 \times 10^{-2}$, $Re_R = 23.4 \times 10^3$, $N = 0.19$ Hz, $r/R = 0.86$.

c. Amplitude $A_s(\xi)$ of the f_s Fourier mode.

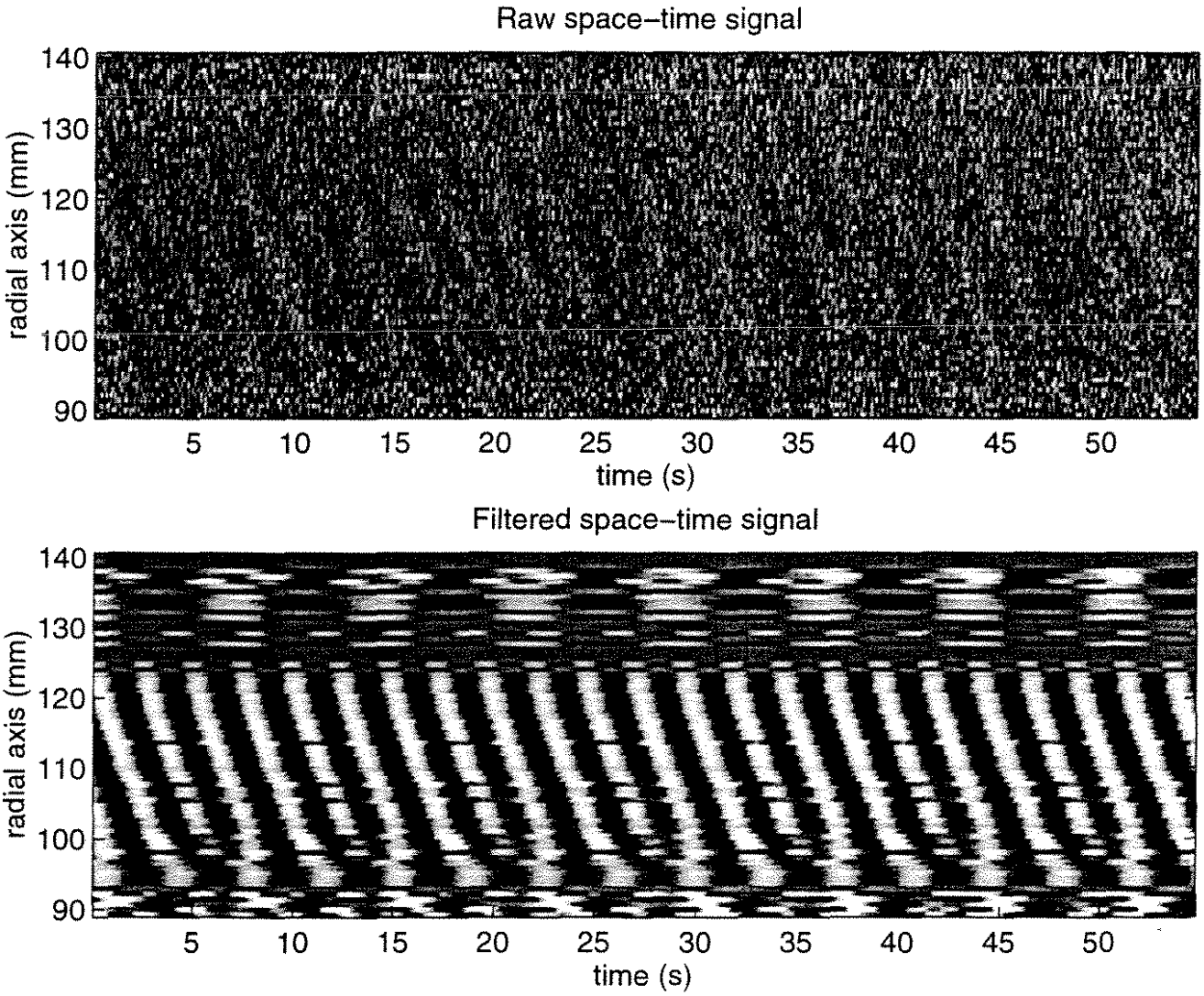

Fig. 7. $v_r(r,t) - \langle v_r(r) \rangle$ for $\gamma = 11.43 \times 10^{-2}$, $Re_R = 17.2 \times 10^3$, $N = 0.14$ Hz. Top : Raw signal, Bottom : Filtered signal.

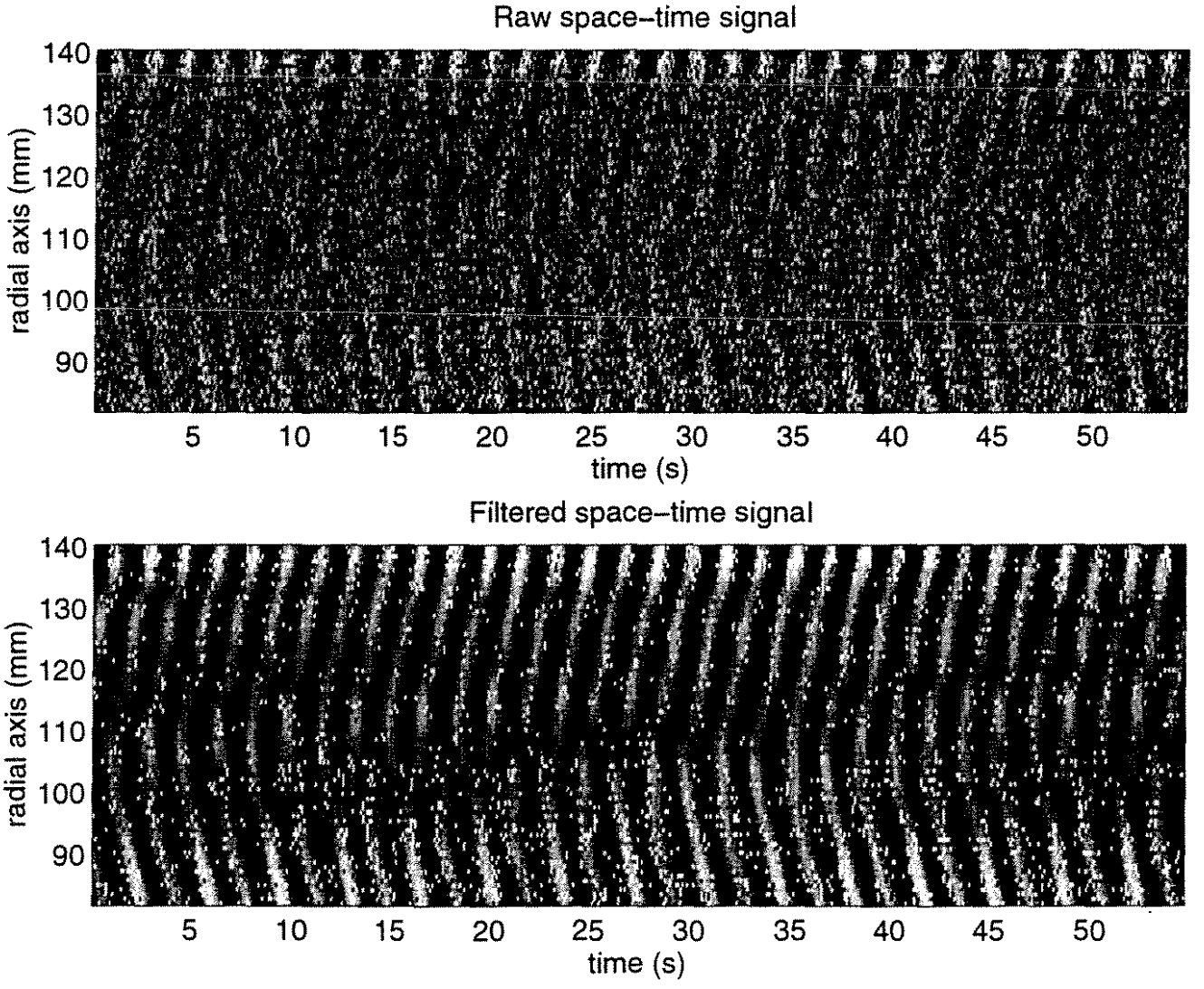

Fig. 8. $v_r(r,t) - \langle v_r(r) \rangle$ for $\gamma = 11.43 \times 10^{-2}$, $Re_R = 34.5 \times 10^3$, $N = 0.28$ Hz. Top : Raw signal, Bottom : Filtered signal.

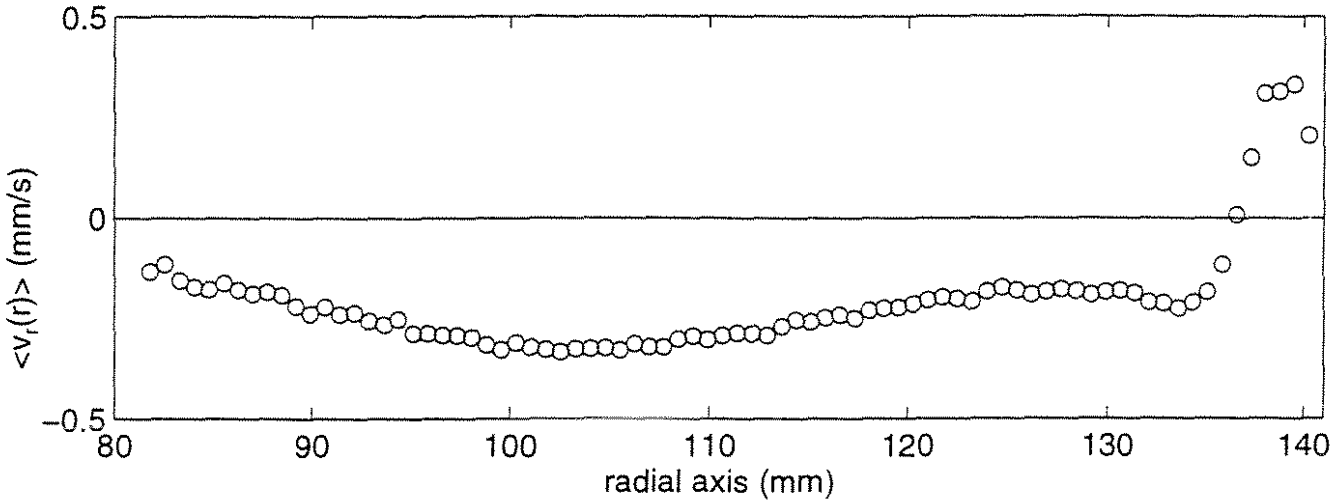

Fig. 9. Temporal mean profile $\langle v_r(r) \rangle$ for $\gamma = 11.43 \times 10^{-2}$ and $Re_R = 17.2 \times 10^3$, $N = 0.14$ Hz.

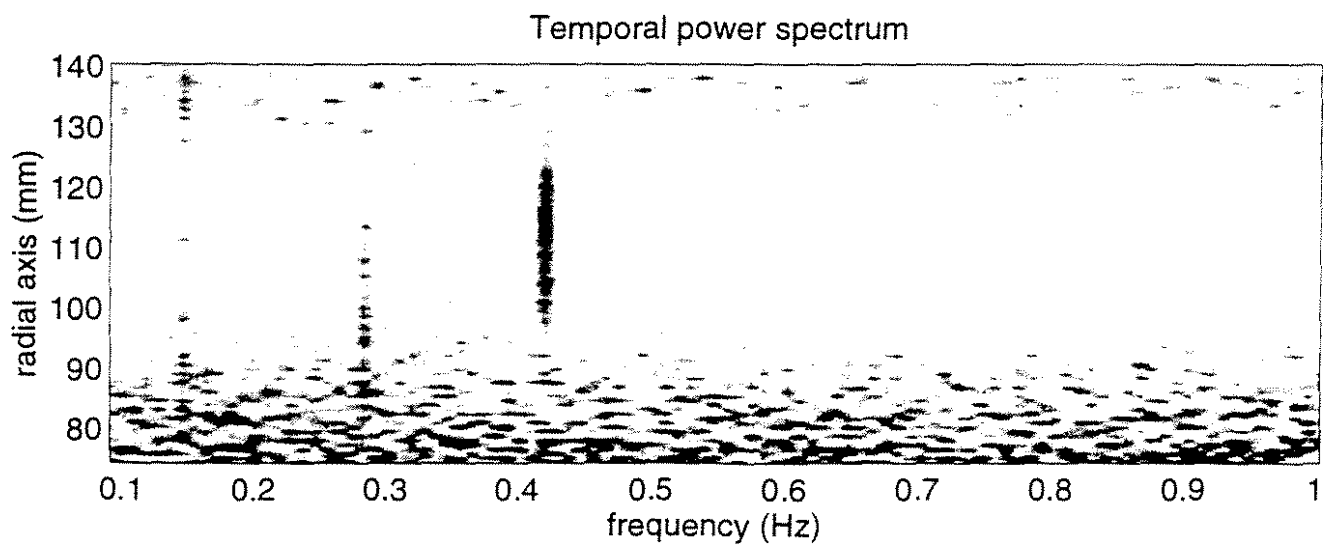

Fig. 10. Temporal power spectrum of $v_r(r,t)$ for $\gamma = 11.43 \times 10^{-2}$ and $Re_R = 17.2 \times 10^3$, $N = 0.14$ Hz.

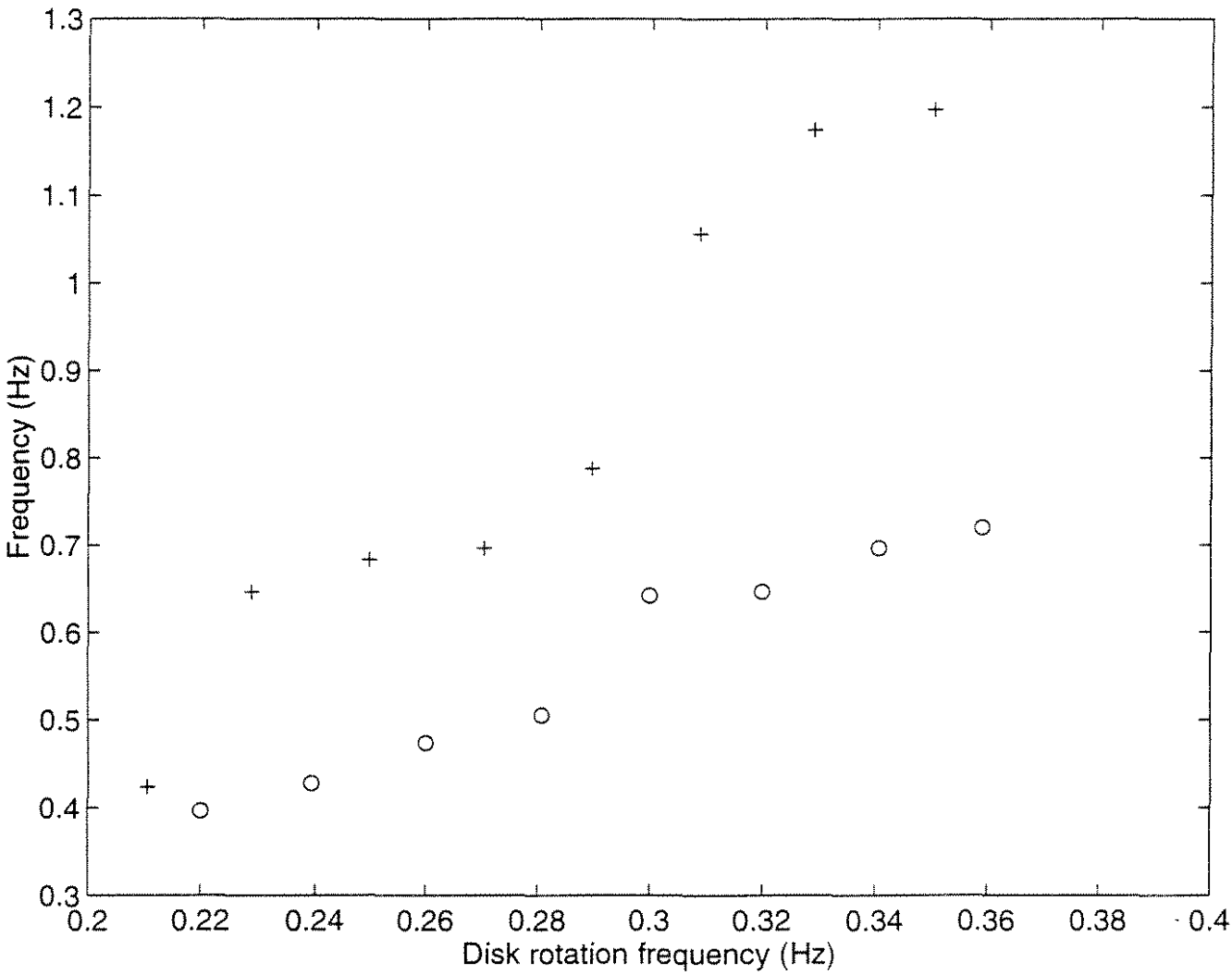

Fig. 12. Evolution of f_s with N : O. increasing, +. decreasing. $\gamma = 11.43 \times 10^{-2}$.

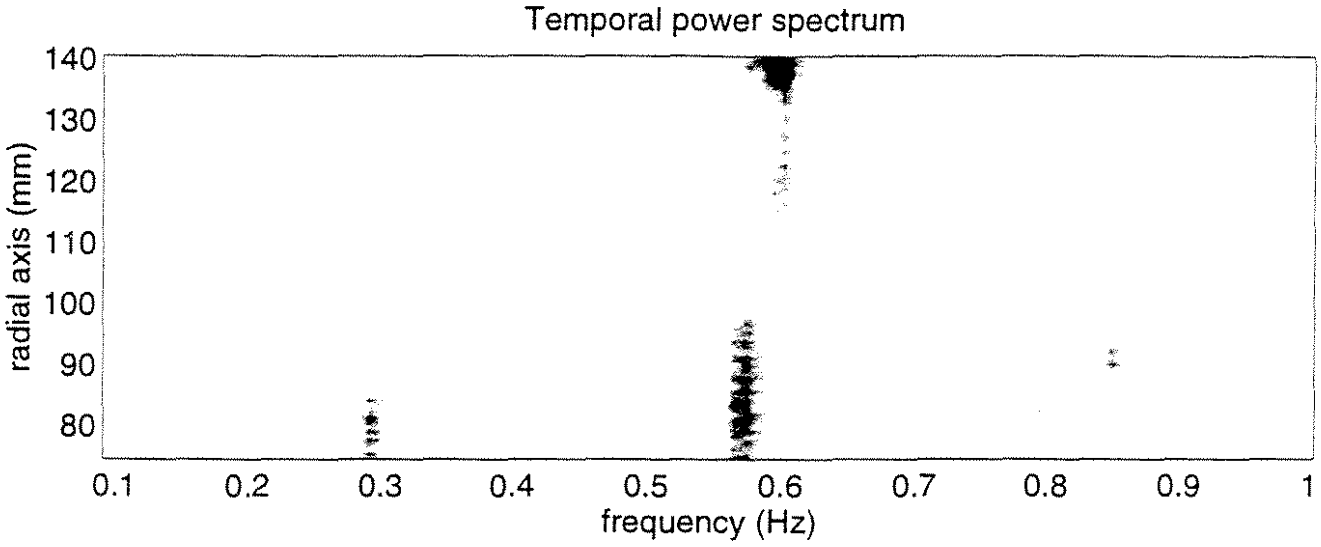

Fig. 11. Temporal power spectrum of $v_r(r,t)$ for $\gamma = 11.43\times10^{-2}$ and $Re_R = 34.5\times10^3$, $N = 0.28$ Hz.

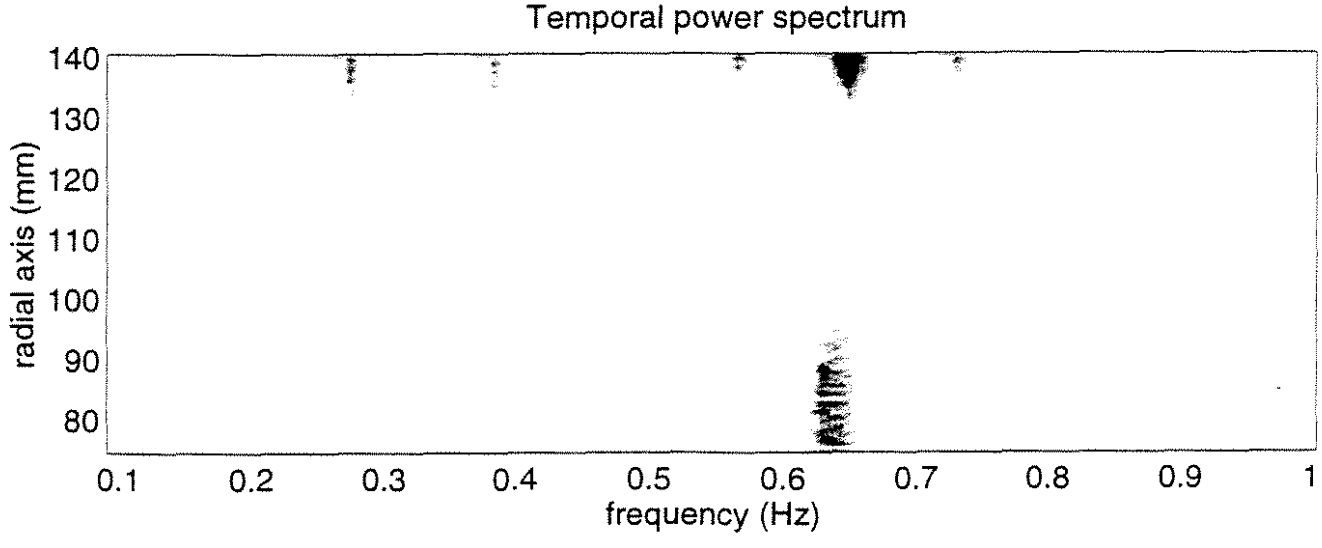

Fig. 13. Temporal power spectrum of $v_r(r,t)$ for $\gamma = 11.43\times10^{-2}$ and $Re_R = 39.4\times10^3$, $N = 0.32$ Hz.